arXiv:1704.00476v1 [cond-mat.mes-hall] 3 Apr 2017

Floquet engineering of long-range p-wave superconductivity: Beyond the high-frequency limit

Zeng-Zhao Li,[1,2,*] Chi-Hang Lam,[3,†] and J. Q. You[2,‡]

[1] *Max Planck Institute for the Physics of Complex Systems, Nöthnitzer Strasse 38, 01187 Dresden, Germany*
[2] *Quantum Physics and Quantum Information Division, Beijing Computational Science Research Center, Beijing 100094, China*
[3] *Department of Applied Physics, Hong Kong Polytechnic University, Hung Hom, Hong Kong, China*

(Dated: April 4, 2017)

It has been shown that long-range p-wave superconductivity in a Kitaev chain can be engineered via an ac field with a high frequency [Benito *et al.*, Phys. Rev. B **90**, 205127 (2014)]. For its experimental realization, however, theoretical understanding of Floquet engineering with a broader range of driving frequencies becomes important. In this work, focusing on the ac-driven tunneling interactions of a Kitaev chain, we investigate effects from the leading correction to the high-frequency limit on the emergent p-wave superconductivity. Importantly, we find new engineered long-range p-wave pairing interactions that can significantly alter the ones in the high-frequency limit at long interaction ranges. We also find that the leading correction additionally generates nearest-neighbor p-wave pairing interactions with a renormalized pairing energy, long-range tunneling interactions, and in particular multiple pairs of Floquet Majorana edge states that are destroyed in the high-frequency limit.

PACS numbers: 03.67.Lx, 75.10.Pq, 03.65.Vf

I. INTRODUCTION

The Floquet engineering, being a promising quantum engineering and quantum control technology, has attracted much attention in recent years. Its main idea is to design appropriate time-periodic driving protocols to engineer properties of a time-independent effective Hamiltonian that governs the time evolution of periodically driven quantum systems. Besides usual properties analogous to their static counterparts, Floquet quantum systems possess additional unique features that result from the periodicity of their quasienergy spectrum. Given the versatility of driving protocols, Floquet engineering opens up new possibilities for exploring and observing exotic phenomena unreachable in static systems[1–15]. For example, this technique has been employed to realize dynamical localization[16–18], photon-assisted tunneling[19–21], and novel topological band structures[22–29].

A promising quantum system for implementing Floquet engineering is a Kitaev chain. It is a one-dimensional p-wave superconducting wire supporting Majorana zero modes at its ends[30] and can potentially be realized in realistic quantum systems such as a quantum nanowire[31–37]. Similar to the static case, a driven Kitaev chain hosts end states called Floquet Majorana zero modes which may realize fault-tolerant quantum computation[38] and also provide a new way to detect these elusive Majorana states[39,40].

Interestingly, a very recent work has demonstrated that long-range p-wave superconductivity (or equivalently long-range many-body spin interactions) can be engineered by periodically driving the tunneling interactions in a Kitaev chain[29]. It has been shown for example that the generated next-neighbor interactions become comparable to the first-neighbor interactions as the driving amplitude increases[29]. These interesting observations, however, are based on the high driving frequency limit. A thorough understanding of Floquet engineering with a broader range of driving frequencies is important for the experimental realization of the effective long-range p-wave superconductivity.

In this work, we consider a driving protocol where the tunneling interactions of a Kitaev chain are modulated by an ac field. We focus on the leading correction to the high-frequency limit. We find that the leading correction results in long-range p-wave pairing interactions with interaction strengths depending nontrivially on the driving amplitude and frequency of the applied ac field. Compared with the ones corresponding to the high-frequency limit, these new interactions become important when the interaction range increases. We also find that the long-range tunneling interactions, the nearest-neighbor pairing interactions, and multiple Floquet Majorana edge states can now be engineered with the leading correction. We believe that our results are important for the experimental realization of Floquet-engineered long-range p-wave pairing interactions and tunneling interactions. They also provide new insights about the quantum engineering of new exotic phases in realistic quantum systems.

This paper is organized as follows. In Sec. II, we introduce a model of a time-dependent Kitaev chain. In Sec. III, we present our driving protocol by considering periodically driven tunneling interactions of a Kitaev chain and derive an effective time-independent Hamiltonian. In Sec. IV, we illustrate the important role that the leading correction plays in the engineered long-range pairing interactions. In Sec. V, we demonstrate that mul-

tiple Floquet Majorana edge states could be engineered when corrections to the high driving frequency limit are included. Discussions and conclusions are finally given in Sec. VI.

II. THE MODEL

The model under our consideration is a Kitaev chain[30] with tunneling interactions which are periodically driven via, for example, gate voltages applied on a quantum wire. The Hamiltonian of this time-dependent Kitaev chain reads[29]

$$\begin{aligned} H\left(t\right) &= \frac{\mu}{2}\sum_{j=1}^{N}(2f_j^{\dagger}f_j-1)-\sum_{j=1}^{N}\frac{w(t)}{2}(f_j^{\dagger}f_{j+1}+f_{j+1}^{\dagger}f_j) \\ &\quad -\sum_{j=1}^{N}\frac{\Delta}{2}(f_j^{\dagger}f_{j+1}^{\dagger}+f_{j+1}f_j), \end{aligned} \tag{1}$$

where μ and Δ are chemical potential and pairing energy, respectively, while $w(t)$ is the time-dependent tunneling strength. $f_j^{\dagger}$ (f_j) is a fermionic operator that creates (annihilates) a fermion on the jth site. N is the number of the sites. The lattice spacing will be set to unity throughout the paper. This model becomes the well-known Kitaev chain if the Hamiltonian in Eq. (1) does not depend on time.

Consider the periodic boundary condition $f_{N+1}=f_1$ and apply the discrete Fourier transformation, $f_k=\frac{1}{\sqrt{N}}\sum_j f_j e^{-ikj}$, Eq. (1) gives the reciprocal-space Hamiltonian

$$H(t)=\sum_{k>0}\Psi_k^{\dagger}H_k(t)\Psi_k, \tag{2}$$

where $\Psi_k^{\dagger}=(f_k^{\dagger},f_{-k})$ is a two-component operator and $H_k(t)$ is the Bogoliubov-de Gennes (BdG) Hamiltonian in the Nambu space given by

$$H_k\left(t\right) = [\mu-\tilde{w}(t)]\sigma_k^z+\tilde{\Delta}\sigma_k^y. \tag{3}$$

Here $\sigma_k^{y(z)}$ is the Pauli matrix, $\tilde{w}(t)=w(t)\cos k$, and $\tilde{\Delta}=\Delta\sin k$. For a static Kitaev chain with $w(t)\equiv w_0$, it is known that there is a topological nontrivial phase when $\mu<w_0$ and a trivial phase if $\mu>w_0$ given that $\Delta>0$[30]. For a dynamical Kitaev chain with the tunneling interactions being periodically driven by an ac field in the limit of a high driving frequency, it has been shown that an interesting effective model with a long-range p-wave superconductivity (or long-range many-body spin interactions) can be generated[29].

III. DRIVING PROTOCOL AND EFFECTIVE HAMILTONIAN OF LONG-RANGE P-WAVE SUPERCONDUCTIVITY

In this section, we present our driving protocol and derive an effective time-independent Hamiltonian in a rotated reference frame[29] which allows the characterization of different topological phases. Specifically, it is an ac field applied to the tunneling strength in Eq. (1) given by

$$w(t) = w_0+\frac{w_1}{2}\cos(\omega t), \tag{4}$$

with w_0 being a constant, $w_1/2$ the driving amplitude, and ω the driving frequency. Then the BdG Hamiltonian given by Eq. (3) becomes

$$H_k\left(t\right) = \{\mu-[w_0+\frac{w_1}{2}\cos(\omega t)]\cos k\}\sigma_k^z+\Delta\sin k\sigma_k^y. \tag{5}$$

To obtain a simple effective time-independent Hamiltonian, we need to find a suitable rotating frame. We define

$$S_k^{\dagger}=e^{-i\frac{w_1}{2\omega}\sin(\omega t)\cos k\sigma_k^z}, \tag{6}$$

so that Eq. (5) is transformed as

$$\tilde{H}_k\left(t\right)=S_k^{\dagger}(t)H_k(t)S_k(t)-iS_k^{\dagger}(t)\frac{\partial S_k(t)}{\partial t}, \tag{7}$$

which gives

$$\begin{aligned} \tilde{H}_k(t) &= [\mu-w_0\cos k]\sigma_k^z \\ &\quad -i\Delta\sin k\sigma_k^+e^{-i\frac{w_1}{\omega}\sin(\omega t)\cos k} \\ &\quad +i\Delta\sin k\sigma_k^-e^{i\frac{w_1}{\omega}\sin(\omega t)\cos k}. \end{aligned} \tag{8}$$

By using the Jacobi-Anger expansion

$$e^{iz\sin\theta}=\sum_{n=-\infty}^{\infty}\mathcal{J}_n(z)e^{in\theta} \tag{9}$$

with $\mathcal{J}_n\left(x\right)$ being the nth-order Bessel function of the first kind, the Hamiltonian $\tilde{H}_k(t)$ becomes

$$\tilde{H}_k(t) = \sum_{p=-\infty}^{\infty}\tilde{H}_{k,p}e^{ip\omega t}, \tag{10}$$

where the Fourier components are given by

$$\begin{aligned} \tilde{H}_{k,p} &= (\mu-w_0\cos k)\sigma_k^z\delta_{p,0}-i\Delta\sin k\sigma_k^+\mathcal{J}_{-p} \\ &\quad +i\Delta\sin k\sigma_k^-\mathcal{J}_p, \end{aligned} \tag{11}$$

with

$$\mathcal{J}_{\pm p}\equiv\mathcal{J}_{\pm p}\left(\frac{w_1}{\omega}\cos k\right). \tag{12}$$

Then one can define the one-period time-evolution operator $U\left(T,0\right)=e^{-i\tilde{H}_k^{\mathrm{eff}}T}$ with the period $T=2\pi/\omega$ and a time-independent effective Hamiltonian $\tilde{H}_k^{\mathrm{eff}}$. Using the Magnus expansion[41] and Eq. (11), the effective

Hamiltonian is expressed as a power series expansion in $1/\omega$[7–9,12], namely

$$\tilde{H}_k^{\rm eff} = \tilde{H}_{k,0} + \frac{1}{\omega}[\tilde{H}_{k,0}, \tilde{H}_{k,1}] - \frac{1}{\omega}[\tilde{H}_{k,0}, \tilde{H}_{k,-1}] - \frac{1}{\omega}[\tilde{H}_{k,-1}, \tilde{H}_{k,1}] + \cdots . \quad (13)$$

The convergence condition for the expansion is $\int_0^T \parallel \tilde{H}_k(t) \parallel dt < \pi$ where $\parallel \cdots \parallel$ denotes the Euclidean norm[29,41].

The previously considered high-frequency limit corresponds to $\omega \to \infty$ in Eq. (13) or equivalently taking only the $p = 0$ term in Eq. (10). In contrast, we also include the leading correction by considering all four terms on the right-hand side of Eq. (13) and obtain an effective BdG Hamiltonian (see Appendix A)

$$\tilde{H}_k^{\rm eff} = \left(\mu - w_0 \cos k + \frac{4\mathcal{J}_0\mathcal{J}_1}{\omega}\Delta^2 \sin^2 k\right)\sigma_k^z + \left[(\mathcal{J}_0 - \frac{4\mu}{\omega})\Delta \sin k + \frac{2w_0\mathcal{J}_1}{\omega}\Delta \sin(2k)\right]\sigma_k^y. \quad (14)$$

Here $\mathcal{J}_0$ and $\mathcal{J}_1$ are given by Eq. (12). This effective Hamiltonian in Eq. (14) reduces to Eq. (31) of Ref. 29 in the high-frequency limit. It contains in particular a pairing term which reads, after summing over the Fourier modes (see also Eq. (A12) in Appendix A),

$$V = -i\sum_{k>0}\Big\{(\mathcal{J}_0 - \frac{4\mu}{\omega})\Delta \sin k + \frac{2w_0\mathcal{J}_1}{\omega}\Delta \sin(2k)\Big\}(f_k^\dagger f_{-k}^\dagger - f_{-k}f_k). \quad (15)$$

To have a better understanding of this effective Hamiltonian, it will be converted to the real space by performing the inverse Fourier transformation. This is however non-trivial due to the k-dependent argument of the Bessel functions. We thus first evaluate the Bessel functions by using the expansions[42,43]

$$\mathcal{J}_0 = \sum_{m=0}^{\infty}\frac{(-1)^m}{(m!)^2}\left(\frac{w_1\cos k}{2\omega}\right)^{2m}, \quad (16)$$

$$\mathcal{J}_1 = \sum_{m=0}^{\infty}\frac{(-1)^m}{m!(m+1)!}\left(\frac{w_1\cos k}{2\omega}\right)^{2m+1}, \quad (17)$$

$$\mathcal{J}_0\mathcal{J}_1 = \sum_{m=0}^{\infty}\frac{(-1)^m(2m+1)}{[m!(m+1)!]^2}\left(\frac{w_1\cos k}{2\omega}\right)^{2m+1}. \quad (18)$$

After substituting into Eq. (14) and performing some simplifications, the effective BdG Hamiltonian becomes

$$\tilde{H}_k^{\rm eff} = \left[\mu - w_0\cos k + \sum_{m=0}^{\infty}\sum_{r=1,3,\cdots}^{2m+3} 2\mathcal{C}_1\mathcal{D}_1\cos(kr)\right]\sigma_k^z + \left[\sum_{m=0}^{\infty}\sum_{r'=1,3,\cdots}^{2m+1} 2\mathcal{C}_2\mathcal{D}_2\sin(kr') - \frac{4\mu\Delta}{\omega}\sin k + \sum_{m=0}^{\infty}\sum_{r=1,3,\cdots}^{2m+3} 2\mathcal{C}_3\mathcal{D}_3\sin(kr)\right]\sigma_k^y, \quad (19)$$

where

$$\mathcal{C}_1 = 2C_{2m+1}^{m-\frac{r-1}{2}} - C_{2m+1}^{m-\frac{r-3}{2}} - C_{2m+1}^{m-\frac{r+1}{2}}, \quad (20)$$

$$\mathcal{C}_2 = C_{2m}^{m-\frac{r'-1}{2}} - C_{2m}^{m-\frac{r'+1}{2}}, \quad (21)$$

$$\mathcal{C}_3 = C_{2m+1}^{m-\frac{r-3}{2}} - C_{2m+1}^{m-\frac{r+1}{2}}, \quad (22)$$

and

$$\mathcal{D}_1 = \frac{\Delta^2}{\omega}\frac{(-1)^m(2m+1)}{[m!(m+1)!]^2}\left(\frac{w_1}{4\omega}\right)^{2m+1}, \quad (23)$$

$$\mathcal{D}_2 = \frac{(-1)^m\Delta}{2(m!)^2}\left(\frac{w_1}{4\omega}\right)^{2m}, \quad (24)$$

$$\mathcal{D}_3 = \frac{w_0\Delta}{\omega}\frac{(-1)^m}{m!(m+1)!}\left(\frac{w_1}{4\omega}\right)^{2m+1}. \quad (25)$$

Here, C_a^b with $b > 0$ is a binomial coefficient and $C_{2m+1}^{-1} = C_{2m+1}^{-2} = C_{2m}^{-1} = 0$. Besides the original $\cos k$-dependent term, the coefficient of σ_k^z in Eq. (19) now attains other terms involving $\cos(kr)$. It will be evident from the real-space Hamiltonian to be derived below that those with $r > 1$ imply long-range tunnelings. In addition, the σ_k^y term in Eq. (19) clearly demonstrates effective superconducting pairing interactions with coefficients $4\mu\Delta\sin k/\omega$, $2\mathcal{C}_2\mathcal{D}_2\sin(kr')$, and $2\mathcal{C}_3\mathcal{D}_3\sin(kr)$. Being independent of $1/\omega$, the term involving $2\mathcal{C}_2\mathcal{D}_2\sin(kr')$ was previously obtained in the high-frequency limit (i.e., $\omega \to \infty$)[29]. However, those involving $4\mu\Delta\sin k/\omega$ and $2\mathcal{C}_3\mathcal{D}_3\sin(kr)$ are proportional to $1/\omega$ and represent the leading corrections to the high frequency limit. In particular, terms involving $2\mathcal{C}_3\mathcal{D}_3\sin(kr)$ provide a correction to those of $2\mathcal{C}_2\mathcal{D}_2\sin(kr')$.

Here are several remarks. For a finite chain with N sites, it is implied that only terms corresponding to $r, r' \leq N$ should be included. In addition, from Eqs. (23) and (25), it is clear that the reported $\mathcal{D}_1$ and $\mathcal{D}_3$ depend on the amplitude w_1, the frequency ω of the driving field and the pairing energy Δ. These nontrivial dependences on the applied electric field may provide flexible controllability. For $\omega \to \infty$, $\mathcal{D}_1$, $\mathcal{D}_2$ and $\mathcal{D}_3$ in general vanish, with a notable exception that $\mathcal{D}_2 = \Delta/2$ at $m = 0$.

We now perform an inverse Fourier transformation to $H^{\rm eff} = \sum_{k>0}\Psi_k^\dagger\tilde{H}_k^{\rm eff}(t)\Psi_k$ with $\tilde{H}_k^{\rm eff}$ given by Eq. (19)

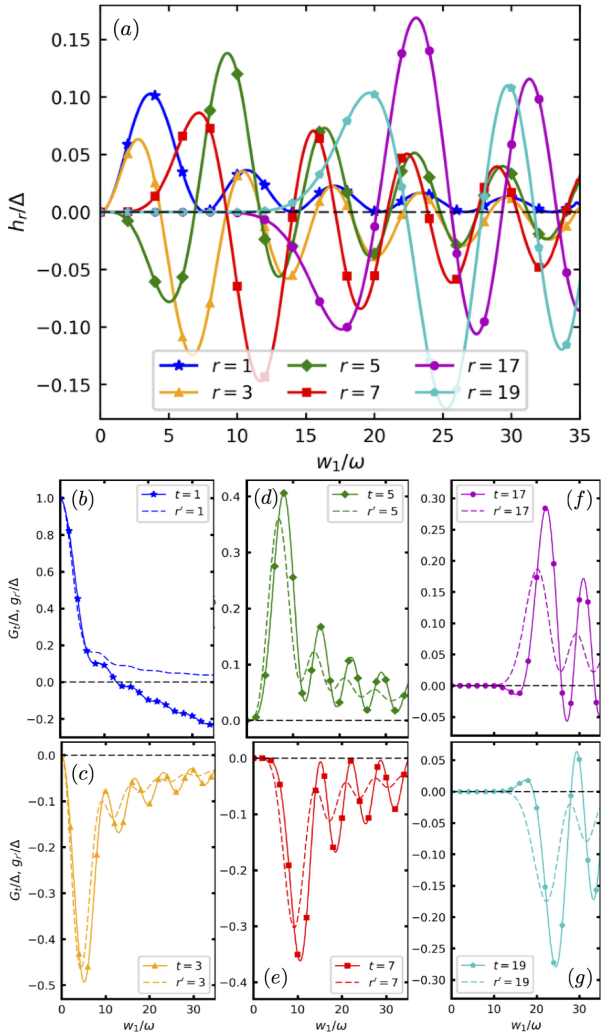

FIG. 1: The superconducting pairing strength (a) h_r/Δ and (b)-(g) $g_{r'}/\Delta$ (dashed curves) without correction and G_t/Δ (solid curves) with correction for different interaction ranges $r, t, r' \in \{1, 3, 5, 7, 17, 19\}$. The parameters are $w_0 = 0.038w_1$ and $\mu = 0.002w_1$.

and obtain

$$\begin{aligned}\tilde{H}^{\text{eff}} &= \sum_j \Big\{ \frac{\mu}{2}(2f_j^\dagger f_j - 1) - \frac{w_0}{2}(f_j^\dagger f_{j+1} + f_{j+1}^\dagger f_j) \\ &+ \frac{2\mu\Delta}{\omega}(f_j^\dagger f_{j+1}^\dagger + f_{j+1} f_j) \\ &+ \sum_{m=0}^{\infty} \sum_{r=1,3,\cdots}^{2m+3} \mathcal{C}_1\mathcal{D}_1(f_j^\dagger f_{j+r} + f_{j+r}^\dagger f_j) \\ &- \sum_{m=0}^{\infty} \sum_{r'=1,3,\cdots}^{2m+1} \mathcal{C}_2\mathcal{D}_2(f_j^\dagger f_{j+r'}^\dagger + f_{j+r'} f_j) \\ &- \sum_{m=0}^{\infty} \sum_{r=1,3,\cdots}^{2m+3} \mathcal{C}_3\mathcal{D}_3(f_j^\dagger f_{j+r}^\dagger + f_{j+r} f_j) \Big\}. \quad (26)\end{aligned}$$

The first two terms in the curly brackets representing the on-site chemical potential and nearest-neighbor tunnelings, are the same as those in the static counterpart of Eq. (1). The fifth term involving $\mathcal{C}_2\mathcal{D}_2$ includes long-range p-wave pairing interactions, e.g., $f_j^\dagger f_{j+r'}^\dagger$ ($r' = 3, 5, \cdots, 2m+1$) and is also present in the high-frequency limit[29].

We now focus on new correction terms of leading order $1/\omega$. One is the third term in the curly brackets in Eq. (26). It represents nearest-neighbor superconducting pairing with a renormalized pairing energy $2\mu\Delta/\omega$ that depends on the driving frequency ω in contrast to a constant bare value of $\Delta/2$ in Eq. (1). The other is the fourth term representing both engineered nearest-neighbor ($r = 1$) and long-range ($r \geq 3$) tunneling $f_j^\dagger f_{j+r}$ with a strength $\mathcal{C}_1\mathcal{D}_1/4$. More interestingly, the sixth term involving $\mathcal{C}_3\mathcal{D}_3 f_j^\dagger f_{j+r}^\dagger/2$ ($r = 1, 3, \cdots, 2m+3$) is the leading correction to the p-wave pairing. These new long-range pairing corrections can both enhance or reduce the pairing interaction strength as demonstrated below. Finally, we emphasize that these corrections are all proportional to $1/\omega$ or its powers and vanish in the high frequency limit.

IV. LONG-RANGE P-WAVE PAIRING

To illustrate that corrections to the high-frequency limit can play an important role in the engineered long-range p-wave superconductivity, we now analyze in detail the pairing strength. Given an interaction range t, the pairing term in Eq. (19) can be written as $V = \sum_t G_t \sin(kt)\sigma_k^y$ with

$$G_t = f_1\delta_{1,t} + g_{r\prime}\delta_{r\prime,t} + h_r\delta_{r,t}, \quad (27)$$

where

$$f_1(\mu) = -\frac{4\mu\Delta}{\omega}, \quad (28)$$

$$g_{r\prime}(w_1) = \sum_{m=0}^{\infty} 2\mathcal{C}_2\mathcal{D}_2, \quad (29)$$

$$h_r(w_1) = \sum_{m=0}^{\infty} 2\mathcal{C}_3\mathcal{D}_3. \quad (30)$$

Here $t, r', r \in \{1, 3, \cdots\}$. Note that $g_{r\prime}(w_1)$ is the only non-vanishing term in the high frequency limit and is identical to the previous result in Ref. 29. In contrast, f_1 and h_r in Eqs. (28) and (30) respectively are corrections reported for the first time in this work. In particular, $h_r (r > 1)$ denotes the long-range pairing correction, at which we are particularly interested.

Figure 1(a) shows that the correction h_r is negligible for small values of $w_1/\omega \ll 1$. However, with the increase of w_1/ω, the individual terms $|h_r|$ increase and further show damping oscillations. The impacts due to the corrections h_r and f_1 are further illustrated in Figs. 1(b)-(g) that show the superconducting pairing strengths G_t and $g_{r\prime}$ with and without corrections, respectively. For

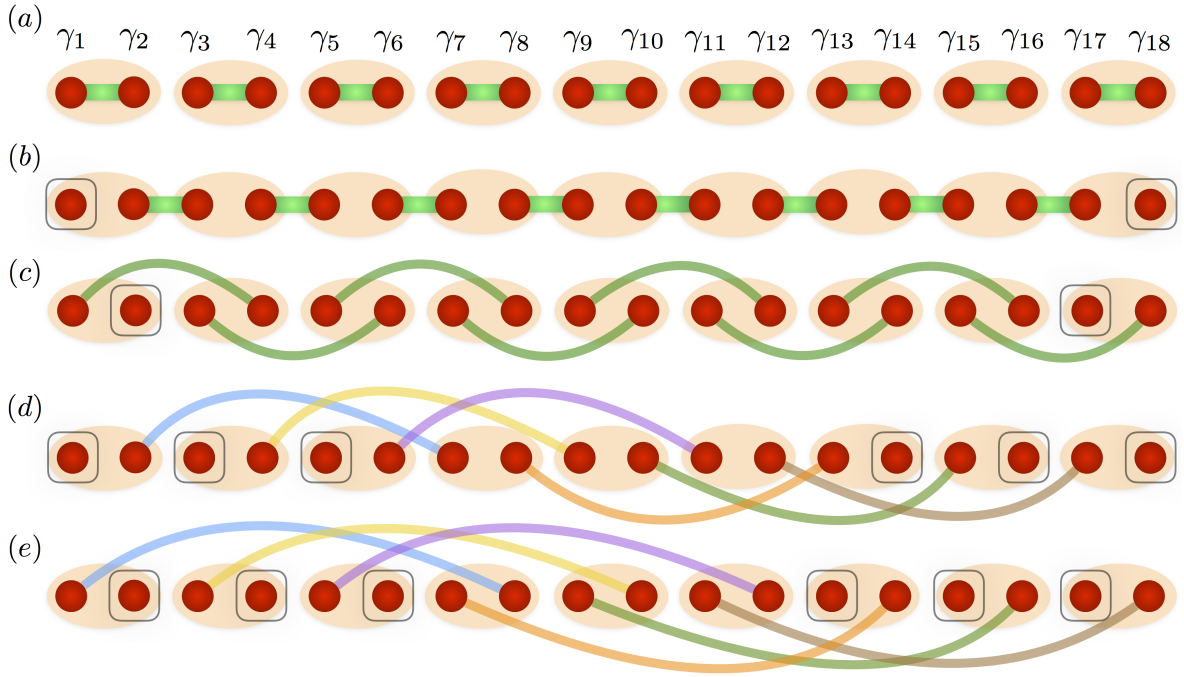

FIG. 2: Schematic diagram of Floquet Majorana edge states. The dominant interaction term and the resulting edge states are (a) $ia_{2j-1}a_{2j}$ and no edge states, (b) $i\gamma_{2j}\gamma_{2j+1}$ and $(\gamma_1,\ \gamma_{2N})$, (c) $i\gamma_{2j-1}\gamma_{2j+2}$ and $(\gamma_2,\ \gamma_{2N-1})$, (d) $i\gamma_{2j}\gamma_{2j+2r-1}$ and $(\gamma_{2l-1}, \gamma_{2N-2(l-1)})$, and (e) $i\gamma_{2j-1}\gamma_{2j+2r}$ and $(\gamma_{2l}, \gamma_{2N-(2l-1)})$ with $1 \le l \le r$ and $r = 1, 3, \cdots$. In order to illustrate the long-range p-wave pairing ($r > 1$), here we consider $r = 3$ and at least $2N = 18$ sites. Note that (a), (b), and (c) also appear for a Kitaev chain with appropriate parameters even without applying an ac field. The box is used to distinguish a decoupled zero-energy Majorana.

the nearest-neighbor pairing interaction with $t = r' = 1$ in Fig. 1(b), G_1 shows a damping washboard behavior and changes from positive to negative in addition to exhibiting damping oscillations, in contrast to g_1 which approaches to zero. Importantly, for the long-range pairing, e.g., $t, r' \ge 3$ in Figs. 1(c)-(g), it is shown that the deviation of $g_{r'}$ from G_t becomes significant when increasing the interaction length, indicating the importance of the correction at long interaction ranges. For example, we clearly observe shifted extremum points and also enhanced magnitudes as the range increases from 7 to 19 in Figs. 1(e) and (g), respectively. It is also shown that long-range pairing interactions $G_t (t > 1)$ attain magnitudes comparable to or beyond that of G_1 for $w_1/\omega \gtrsim 1$. Interestingly, we also find that there are regimes where one long-range pairing strength can be larger than that of the other ranges, e.g., $|G_7| > |G_t|$ $(t \ne 7)$, implying the possibility of the engineering of a predominantly arbitrarily-ranged pairing interaction. In a nutshell, the long-range pairing corrections are crucial for any detectable long-range p-wave superconductivity.

V. FLOQUET MAJORANA EDGE STATES

Although the long-range p-wave pairing was reported previously in the limit of a high driving frequency (i.e., $\omega \to \infty$), edge states and their observability were not discussed[29]. In this section, we are going to show that the leading correction of order $1/\omega$ gives rise to multiple pairs of Floquet Majorana edge states which, however, are destroyed in the high-frequency limit.

Considering open boundary conditions and applying Majorana operators

$$\gamma_{2j-1} = f_j + f_j^\dagger, \quad \gamma_{2j} = -i(f_j - f_j^\dagger), \tag{31}$$

Eq. (26) is represented as

$$\begin{aligned}\tilde{H}^{\rm eff} \;=\; & \sum_j \Big\{ \frac{\mu}{2} i\gamma_{2j-1}\gamma_{2j} + \frac{w_0\omega - 4\mu\Delta}{4\omega} i\gamma_{2j}\gamma_{2j+1} \\ & - \frac{w_0\omega + 4\mu\Delta}{4\omega} i\gamma_{2j-1}\gamma_{2j+2} \\ & - \sum_{m=0}^{\infty} \Big[\sum_{r=1,3,\cdots}^{2m+3} \Big(\frac{\mathcal{C}_1\mathcal{D}_1 - \mathcal{C}_3\mathcal{D}_3}{2} i\gamma_{2j}\gamma_{2j+2r-1} \\ & - \frac{\mathcal{C}_1\mathcal{D}_1 + \mathcal{C}_3\mathcal{D}_3}{2} i\gamma_{2j-1}\gamma_{2j+2r} \Big) \\ & - \sum_{r'=1,3,\cdots}^{2m+1} \frac{\mathcal{C}_2\mathcal{D}_2}{2} i\Big(\gamma_{2j}\gamma_{2j+2r'-1} + \gamma_{2j-1}\gamma_{2j+2r'} \Big) \Big] \Big\}. \end{aligned} \tag{32}$$

A. High-frequency limit

In order to better understand the important role that the leading correction plays in the generation of detectable Majorana edge states, let us first start with the high-frequency limit. The above Hamiltonian in Eq. (32) is further simplified to

$$\tilde{H}^{\rm eff} = \sum_j \Big\{ \frac{\mu}{2} i\gamma_{2j-1}\gamma_{2j} + \frac{w_0}{4} i\Big(\gamma_{2j}\gamma_{2j+1} - \gamma_{2j-1}\gamma_{2j+2}\Big) + \sum_{r'=1,3,\cdots}^{2m+1} \frac{\mathcal{C}_2\mathcal{D}_2}{2} i\Big(\gamma_{2j}\gamma_{2j+2r'-1} + \gamma_{2j-1}\gamma_{2j+2r'}\Big)\Big]\Big\}. \tag{33}$$

In the second term on the right-hand side of Eq. (33), two Majoranas γ_1 and γ_{2N} that are absent from the interaction $i\gamma_{2j}\gamma_{2j+1}$ (see Fig. 2(b)) are however coupled via the interaction $i\gamma_{2j-1}\gamma_{2j+2}$ to γ_4 and γ_{2N-3} (see Fig. 2(c)), respectively. These couplings destroy the Majoranas. Also, γ_2 and γ_{2N-1} absent from $i\gamma_{2j-1}\gamma_{2j+2}$ (see Fig. 2(c)) are coupled via the interaction $i\gamma_{2j}\gamma_{2j+1}$ to γ_3 and γ_{2N-2} (see Fig. 2(b)), respectively. Due to the third term in Eq. (33), Majorana pairs $(\gamma_{2l-1}, \gamma_{2N-2(l-1)})$ with $1 \le l \le r'$, i.e., $\gamma_1, \gamma_3, \cdots, \gamma_{2r'-1}$ on one end of the chain and $\gamma_{2N-2(r'-1)}, \cdots, \gamma_{2N-2}, \gamma_{2N}$ on the other end (see Fig. 2(d) where $r' = 3$ and $2N = 18$), which are not coupled by $i\gamma_{2j}\gamma_{2j+2r'-1}$, are on the other hand coupled by $i\gamma_{2j-1}\gamma_{2j+2r'}$. Similarly, for the interaction $i\gamma_{2j-1}\gamma_{2j+2r'}$, we have Majorana pairs $(\gamma_{2l}, \gamma_{2N-(2l-1)})$, namely, $\gamma_2, \gamma_4, \cdots, \gamma_{2r'}$ on one end and $\gamma_{2N-(2r'-1)}, \cdots, \gamma_{2N-3}, \gamma_{2N-1}$ on the other end as shown in Fig. 2(e), which, however, are coupled by the interaction $i\gamma_{2j}\gamma_{2j+2r'-1}$. The unavoidable destruction of Majorana edge states according to the above analysis essentially results from the same strengths for two kinds of interactions. When the second and third terms are comparable in magnitudes, it is possible to have two unequal coupling strengths $\mathcal{C}_2\mathcal{D}_2/2 + w_0/4$ and $\mathcal{C}_2\mathcal{D}_2/2 - w_0/4$ with $r' = 1$ for interactions $i\gamma_{2j}\gamma_{2j+1}$ and $i\gamma_{2j-1}\gamma_{2j+2}$, respectively, implying that there would be a single Majorana pair (γ_1, γ_{2N}) or $(\gamma_2, \gamma_{2N-1})$ as indicated by the blue dot in Fig. 3(a) (discussions about Fig. 3(a) are given below). As a result, in the high-frequency limit with equal long-range interaction strengths (e.g., $\mathcal{C}_2\mathcal{D}_2/2$ for $r' > 1$), there cannot exist multiple pairs of Floquet Majorana edge states.

B. Beyond the high driving frequency

We now go back to consider Eq. (32) that includes the leading correction and therefore goes beyond the high driving frequency limit. Let us first consider the second and third terms inside the curly brackets in Eq. (32). Performing similar analysis to that on Eq. (33), we know that it is possible to have two Majorana edge states γ_1 and γ_{2N} if $w_0\omega \approx -4\mu\Delta$ or γ_2 and γ_{2N-1} if $w_0\omega \approx 4\mu\Delta$,

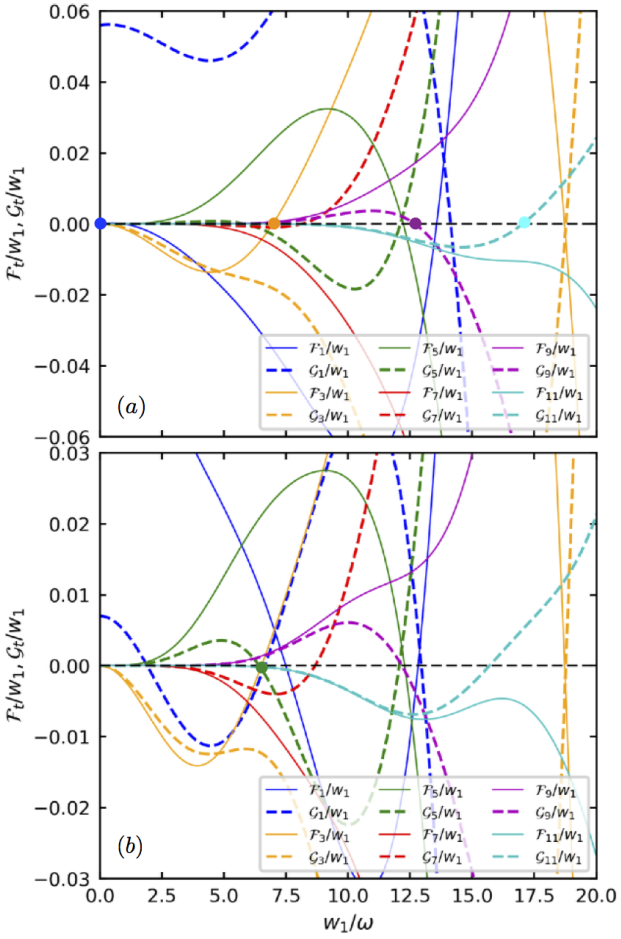

FIG. 3: The coupling strengths $\mathcal{F}_t$ and $\mathcal{G}_t$ for interactions $i\gamma_{2j-1}\gamma_{2j+2t}$ and $i\gamma_{2j}\gamma_{2j+2t-1}$ respectively as a function of w_1/ω. The blue dot in (a) indicates a single Floquet Majorana pair while other dots represent the solutions to the equations $\mathcal{F}_t\mathcal{G}_t = 0$ and $\mathcal{F}_t + \mathcal{G}_t \neq 0$ necessary for the existence of multiple Majorana pairs. The green dot in (b) denotes the existence of multiple pairs of Floquet Majorana states. We take $w_0 = 0.028w_1$, $\mu = -0.01w_1$ in (a) and $w_0 = -0.021w_1$, $\mu = -0.00001w_1$ in (b). Other parameter is $\Delta = 0.028w_1$.

as shown in Fig. 2(b) or (c) respectively. This simple condition for having Majoranas is based on the assumption of negligible contributions from the fourth, fifth and sixth terms with $r = r' = 1$. When the fourth and fifth terms including long-range interactions (e.g., $r \ge 3$) become dominant, there would be multiple Majorana pairs $(\gamma_{2l-1}, \gamma_{2N-2(l-1)})$ if $\mathcal{C}_1\mathcal{D}_1 \approx -\mathcal{C}_3\mathcal{D}_3$ and $(\gamma_{2l}, \gamma_{2N-(2l-1)})$ if $\mathcal{C}_1\mathcal{D}_1 \approx \mathcal{C}_3\mathcal{D}_3$ ($1 \le l \le r$ with $r = 1, 3, \cdots, 2m+3$).

Similar to the analyses above, we can extract from Eq. (32) a general condition for the existence of Floquet Majorana edge states. The coupling strengths for interactions $i\gamma_{2j-1}\gamma_{2j+2t}$ and $i\gamma_{2j}\gamma_{2j+2t-1}$ are defined by $\mathcal{F}_t$ and $\mathcal{G}_t$ respectively, which are given by

$$\mathcal{F}_t = G_t + F_t, \tag{34}$$
$$\mathcal{G}_t = G_t - F_t, \tag{35}$$

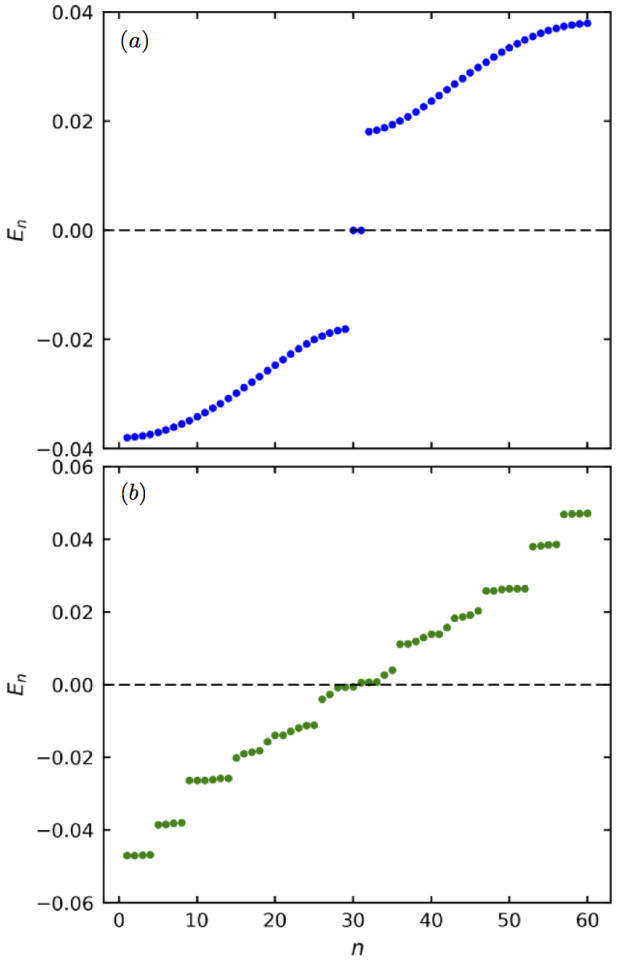

FIG. 4: The energy spectrum of the effective Hamiltonian (i.e., Eq. (26)) with $N = 30$ sites. We take $w_1/\omega = 0.001$ in (a) and 6.989 in (b) corresponding to the blue and green dots in Fig. 3(a) and (b) respectively. Other parameters are same as those in Fig. 3.

where the pairing strength G_t is given by Eq. (27) and the tunneling strength F_t is defined as

$$F_t = p_1\delta_{1,t} + q_r\delta_{r,t}, \tag{36}$$

with

$$p_1 = -w_0, \tag{37}$$

$$q_r(w_1) = \sum_{m=0}^{\infty} 2\mathcal{C}_1\mathcal{D}_1. \tag{38}$$

Therefore, Majorana edge states are indicated by the solutions to equations $\mathcal{F}_t\mathcal{G}_t = 0$ and $\mathcal{F}_t + \mathcal{G}_t \neq 0$. If $\mathcal{F}_t = 0$ and $\mu \ll |\mathcal{G}_t| \neq 0$, we have Majorana edge states γ_{2l-1} and $\gamma_{2N-2(l-1)}$. Alternatively, if $\mu \ll |\mathcal{F}_t| \neq 0$ and $\mathcal{G}_t = 0$, the edge states become γ_{2l} and $\gamma_{2N-(2l-1)}$ with $1 \leq l \leq t$.

Figure 3 shows how coupling strengths $\mathcal{F}_t$ and $\mathcal{G}_t$ vary as w_1/ω increases. We find that there are solutions to the above-mentioned equations, i.e., $\mathcal{F}_t\mathcal{G}_t = 0$ and $\mathcal{F}_t + \mathcal{G}_t \neq 0$, as indicated by dots in Fig. 3(a). The color of the dot denotes the number of Floquet Majorana pairs corresponding to the range of the p-wave pairing interaction. Figure 3(a) shows clearly that a single pair of Majoranas i.e., (γ_1, γ_{2N}) indicated by the blue dot exists in the high-frequency limit, i.e., $w_1/\omega \to 0$. This single Majorana pair is further confirmed by the zero-energy modes of the effective Hamiltonian (i.e., Eq. (26)), as demonstrated in Fig. 4(a), and also by the exponential decay of the spatial profile of Majorana operators in Figs. 5(a1) and (a2). In addition, we find that multiple Majorana pairs are not stable. For example, nine pairs of Majoranas $(\gamma_{2l}, \gamma_{2N-(2l-1)})$ with $1 \leq l \leq 9$ represented by the purple dot in Fig. 3(a) would be destroyed by the inevitable interaction e.g., $i\gamma_{2j}\gamma_{2j+1}$ (or $i\gamma_{2j-1}\gamma_{2j+2}$) due to $\mathcal{F}_9 < \mathcal{G}_1$ (or $\mathcal{F}_9 < |\mathcal{F}_1|$) at the corresponding w_1/ω.

In order to have stable Majorana pairs, an additional condition e.g., $|\mathcal{G}_t| > |\mathcal{G}_{t'}|$ $(t' < t)$ and $|\mathcal{G}_t| > |\mathcal{F}_{t''}|$ $(t'' \neq t)$ when $\mathcal{F}_t = 0$ or $|\mathcal{F}_t| > |\mathcal{F}_{t'}|$ $(t' < t)$ and $|\mathcal{F}_t| > |\mathcal{G}_{t''}|$ $(t'' \neq t)$ when $\mathcal{G}_t = 0$ should be fulfilled. By using different parameters i.e., $w_0 = -0.021\omega_1$ and $\mu = -0.00001w_1$ from those in Fig. 3(a), it is shown in Fig. 3(b) that the green dot indicates $\mathcal{G}_5 = \mathcal{F}_3 = \mathcal{G}_1 = 0$ and $\mathcal{F}_5 > |\mathcal{G}_3| > \mathcal{F}_1$, implying that there might be five pairs of Floquet Majorana states. Using the corresponding driving field, i.e., $w_1/\omega = 6.989$ for the green dot, the energy spectrum of the effective Hamiltonian (i.e., Eq. (26)) in Fig. 4(b) does show multiple Floquet Majorana pairs with $E_n \sim 0$.

To further verify the existence of multiple pairs of Floquet Majorana states beyond the high driving frequency limit, we calculate the spatial profile i.e., $\varphi^n_{N-i} + (\phi^n_{N-i})^*$ and $\varphi^n_{N-i} - (\phi^n_{N-i})^*$ $(i = 0, 1, 2, 3, 4$ and $n = 1, 2, \cdots, N)$ of Majorana operators $\gamma_{n,+} = \sum_j [\varphi^n_j + (\phi^n_j)^*]f_j + [\phi^n_i + (\varphi)^*]f^\dagger_j$ and $\gamma_{n,-} = -i\sum_j [\varphi^n_j - (\phi^n_j)^*]f_j + [\phi^n_j - (\varphi^n_j)^*]f^\dagger_j$[44]. Here φ^n_j and ϕ^n_j are coefficients used to define the operators $\psi_n = \sum_j \varphi^n_j f_j + \phi^n_j f^\dagger_j$ which together with $\psi^\dagger_n$ diagonalize the effective Hamiltonian in Eq. (26), namely, $\tilde{H}^{\text{eff}} = \sum_n E_n(\psi^\dagger_n\psi_n - \psi_n\psi^\dagger_n)/2$. Figure 5(a1) and (a2) show the spatial profile (i.e., $\varphi^n_N + (\phi^n_N)^*$ and $\varphi^n_N - (\phi^n_N)^*$ with $N = 30$) of a single Majorana pair corresponding to the energy spectrum in Fig. 4(a) and the blue dot in Fig. 3(a). In contrast to this well-known exponential decay starting from the edges in Fig. 5(a1) and (a2), the drastically different spatial profiles of Majorana operators are observed in Figs. 5(b1)-(f2) verifying the existence of multiple pairs of Floquet Majorana states indicated already by the energy spectrum in Fig. 4(b) and the green dot in Fig. 3(b).

It is expected that many more pairs of Majoranas could also be achievable by choosing different parameters. We emphasize that our reported conditions for the existence of multiple Floquet Majorana edge states can be realized by properly tuning the parameters such as the driving frequency ω and the amplitude w_1 of the applied ac field.

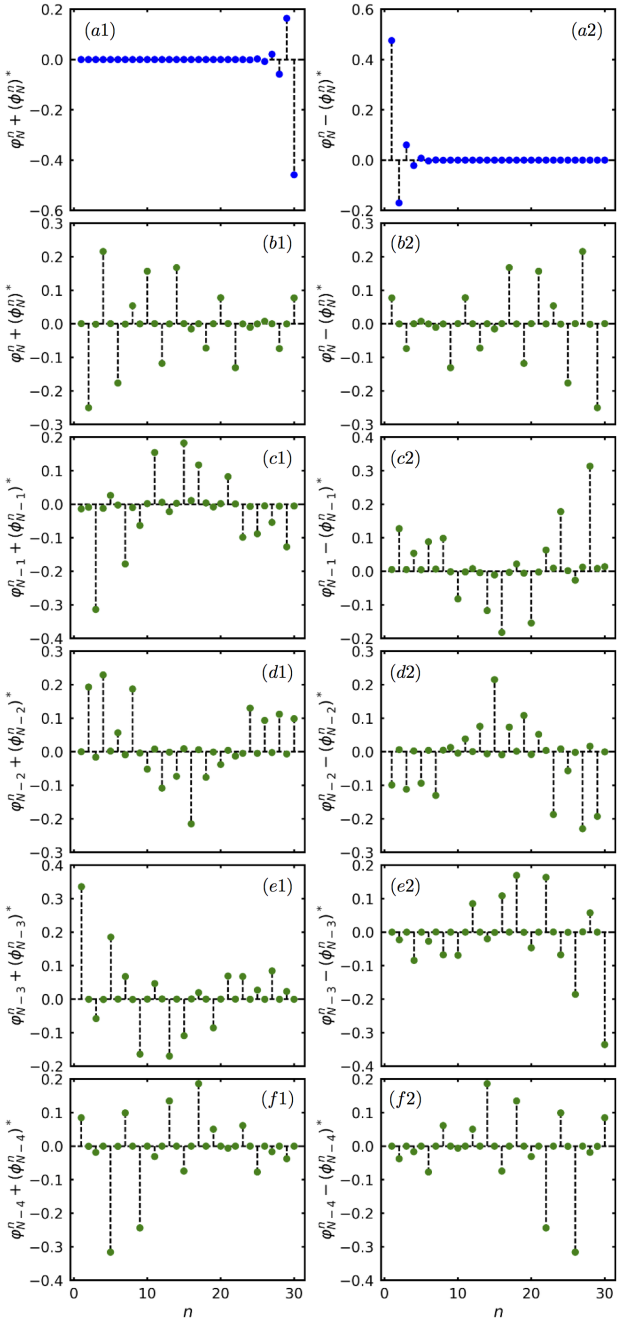

FIG. 5: The spatial profile $\varphi^n_{N-i} + (\phi^n_{N-i})^*$ and $\varphi^n_{N-i} - (\phi^n_{N-i})^*$ with $i = 0, 1, 2, 3, 4$ and $N = 30$ of Majorana operators $\gamma_{n,\pm}$. (a1) and (a2) are for a single Majorana pair corresponding to zero-energy modes i.e., $E_{30} = E_{31} = 0$ in Fig. 4(a) while (b1)-(f2) for multiple pairs of Floquet Majorana states corresponding to five pairs of modes close to zero energy in Fig. 4(b).

VI. DISCUSSIONS AND CONCLUSIONS

Given the known correspondence between the Kitaev chain and the one dimensional transverse Ising model[45], there is an effective spin representation for our effective Hamiltonian obtained above. Specifically, we apply the inverse Jordan-Wigner transformation[46,47] $\sigma_j^+ = f_j^\dagger \prod_{m=1}^{j-1}(2f_m^\dagger f_m - 1)$ and $\sigma_j^- = \prod_{m=1}^{j-1}(2f_m^\dagger f_m - 1) f_j$ on Eq. (26) and obtain an equivalent Hamiltonian in terms of spin operators, namely,

$$\begin{aligned}\tilde{H}^{\rm eff} &= \sum_j \Big\{ -\frac{\mu}{2}\sigma_j^x - \frac{w_0}{4}(\sigma_j^y\sigma_{j+1}^y + \sigma_j^z\sigma_{j+1}^z) \\ &+\frac{\mu\Delta}{\omega}(\sigma_j^z\sigma_{j+1}^z - \sigma_j^y\sigma_{j+1}^y) \\ &+\sum_{m=0}^{\infty}\sum_{r=1,3,\cdots}^{2m+3}\frac{\mathcal{C}_1\mathcal{D}_1}{2}(\sigma_j^y M_{j,r}^x\sigma_{j+r}^y + \sigma_j^z M_{j,r}^x\sigma_{j+r}^z) \\ &-\sum_{m=0}^{\infty}\sum_{r'=1,3,\cdots}^{2m+1}\frac{\mathcal{C}_2\mathcal{D}_2}{2}(\sigma_j^z M_{j,r'}^x\sigma_{j+r'}^z - \sigma_j^y M_{j,r'}^x\sigma_{j+r'}^y) \\ &-\sum_{m=0}^{\infty}\sum_{r=1,3,\cdots}^{2m+3}\frac{\mathcal{C}_3\mathcal{D}_3}{2}(\sigma_j^z M_{j,r}^x\sigma_{j+r}^z - \sigma_j^y M_{j,r}^x\sigma_{j+r}^y)\Big\},\end{aligned} \tag{39}$$

where

$$M_{j,\chi}^x = \prod_{m=j+1}^{j+\square-1}\sigma_m^x,\ \chi = r, r'. \tag{40}$$

It shows long-range many-body spin interactions with strengths $\mathcal{C}_1\mathcal{D}_1/2$, $\mathcal{C}_2\mathcal{D}_2/2$, and $\mathcal{C}_3\mathcal{D}_3/2$ that correspond to long-range tunneling and pairing interactions in Eq. (26). Note that the spin interactions involving $\mathcal{C}_1$ and $\mathcal{C}_3$, and the nearest-neighbor spin interaction with the strength $\mu\Delta/\omega$ are leading corrections to the high-frequency limit.

We believe that it is possible to observe experimentally the effects of the driving frequency away from the high frequency limit on the Floquet engineering of long-range p-wave superconductivity and Floquet Majorana edge states deduced in this work. This is because the tunneling of carriers can in general be tuned via the gate voltages in quantum-transport experiments. Possible physical realizations include a ferromagnetic atomic chain on a superconductor[35], a one-dimensional wire with Rashba spin-orbit interaction[37], and a semiconductor quantum dot coupled to superconducting grains[48].

We have studied the effects of the leading correction in terms of the inverse driving frequency on the Floquet engineering of long-range p-wave superconductivity in a Kitaev chain. We find that the leading corrections can generate new long-range p-wave pairing interactions, which could appreciably correct the ones present at the high-frequency limit when the interaction range increases. We also find that long-range tunneling interactions and nearest-neighbor p-wave pairings can be generated when applying a broad range of driving frequencies. In addition, we show the leading corrections can give detectable multiple pairs of Floquet Majorana edge states that is destroyed at the high driving frequency limit.

Acknowledgments

ZZL thanks Yong-Chang Zhang and Sheng-Wen Li for very helpful discussions. We acknowledge support from the National Natural Science Foundation of China Grant No. 11404019 and HK PolyU Grant No. G-YBHY.

Appendix A: Derivation of Eq. (14)

The Fourier components given in Eq. (11) for $p = 0, \pm 1$ become

$$\tilde{H}_{k,0} = \mathcal{A}\sigma_k^z - i\mathcal{B}\mathcal{J}_0\sigma_k^+ + i\mathcal{B}\mathcal{J}_0\sigma_k^-, \quad \text{(A1)}$$

$$\tilde{H}_{k,1} = -i\mathcal{B}\mathcal{J}_{-1}\sigma_k^+ + i\mathcal{B}\mathcal{J}_1\sigma_k^-, \quad \text{(A2)}$$

$$\tilde{H}_{k,-1} = -i\mathcal{B}\mathcal{J}_1\sigma_k^+ + i\mathcal{B}\mathcal{J}_{-1}\sigma_k^-, \quad \text{(A3)}$$

where

$$\mathcal{A} = \mu - w_0\cos k, \quad \text{(A4)}$$

$$\mathcal{B} = \Delta\sin k, \quad \text{(A5)}$$

$$\mathcal{J}_0 \equiv \mathcal{J}_0\left(\frac{w_1}{\omega}\cos k\right), \quad \text{(A6)}$$

$$\mathcal{J}_{\pm 1} \equiv \mathcal{J}_{\pm 1}\left(\frac{w_1}{\omega}\cos k\right). \quad \text{(A7)}$$

Their commutators are obtained as

$$\left[\tilde{H}_{k,0}, \tilde{H}_{k,1}\right] = -2\mathcal{A}\mathcal{B}\mathcal{J}_1\sigma_k^y + 2\mathcal{B}^2\mathcal{J}_0\mathcal{J}_1\sigma_k^z, \quad \text{(A8)}$$

$$\left[\tilde{H}_{k,0}, \tilde{H}_{k,-1}\right] = 2\mathcal{A}\mathcal{B}\mathcal{J}_1\sigma_k^y - 2\mathcal{B}^2\mathcal{J}_0\mathcal{J}_1\sigma_k^z, \quad \text{(A9)}$$

$$\left[\tilde{H}_{k,1}, \tilde{H}_{k,-1}\right] = 0. \quad \text{(A10)}$$

Here, we have used $[\sigma_k^z, \sigma_k^+] = 2\sigma_k^+$, $[\sigma_k^z, \sigma_k^-] = -2\sigma_k^-$, $[\sigma_k^+, \sigma_k^-] = \sigma_k^z$, and $\mathcal{J}_{-1} = -\mathcal{J}_1$. Inserting these commutators into Eq. (13), we have

$$\begin{aligned}\tilde{H}_k^{\text{eff}} &= \tilde{H}_{k,0} + \frac{1}{\omega}\{[\tilde{H}_{k,0}, \tilde{H}_{k,1}] - [\tilde{H}_{k,0}, \tilde{H}_{k,-1}] \\ &\quad + [\tilde{H}_{k,1}, \tilde{H}_{k,-1}]\} \\ &= \mathcal{A}\sigma_k^z + i\mathcal{B}\left[\mathcal{J}_0 - \frac{4}{\omega}\mathcal{A}\mathcal{J}_1\right](\sigma_k^- - \sigma_k^+) \\ &\quad + \frac{4}{\omega}\mathcal{B}^2\mathcal{J}_0\mathcal{J}_1\sigma_k^z. \end{aligned} \quad \text{(A11)}$$

Further inserting the expressions of $\mathcal{A}$ and $\mathcal{B}$, the effective Hamiltonian in Eq. (14) is then obtained. Using $\tilde{H}^{\text{eff}} = \sum_{k>0}\Psi_k^\dagger\tilde{H}_k^{\text{eff}}\Psi_k$, the Hamiltonian in the reciprocal space becomes

$$\begin{aligned}\tilde{H}^{\text{eff}} &= \sum_{k>0}\Big\{\Big(\mu - w_0\cos k + \frac{4\mathcal{J}_0\mathcal{J}_1}{\omega}\Delta^2\sin^2 k\Big) \\ &\quad \times\Big(f_k^\dagger f_k - f_{-k}f_{-k}^\dagger\Big) - i\Big[\Big(\mathcal{J}_0 - \frac{4\mu}{\omega}\Big)\Delta\sin k \\ &\quad + \frac{2w_0\mathcal{J}_1}{\omega}\Delta\sin(2k)\Big]\Big(f_k^\dagger f_{-k}^\dagger - f_{-k}f_k\Big)\Big\}. \end{aligned} \quad \text{(A12)}$$

* Electronic address: zengzhao@pks.mpg.de
† Electronic address: C.H.Lam@polyu.edu.hk
‡ Electronic address: jqyou@csrc.ac.cn

[1] T. Kitagawa, E. Berg, M. Rudner, and E. Demler, Topological characterization of periodically driven quantum systems, Phys. Rev. B **82**, 235114 (2010).
[2] M. S. Rudner, N. H. Lindner, E. Berg, and M. Levin, Anomalous edge states and the bulk-edge correspondence for periodically driven two-dimensional systems, Phys. Rev. X **3**, 031005 (2013).
[3] L. Jiang et al., Majorana fermions in equilibrium and in driven cold-atom quantum wires, Phys. Rev. Lett. **106**, 220402 (2011).
[4] T. Kitagawa et al., Observation of topologically protected bound states in photonic quantum walks, Nat. Commun. **3**, 882 (2012).
[5] A. Kundu and B. Seradjeh, Transport signatures of Floquet Majorana fermions in driven topological superconductors, Phys. Rev. Lett. **111**, 136402 (2013).
[6] Q. J. Tong, J. H. An, J. Gong, H. G. Luo, and C. H. Oh, Generating many Majorana modes via periodic driving: A superconductor model, Phys. Rev. B **87**, 201109 (2013).
[7] M. Bukov, L. D'Alessio, and A. Polkovnikov, Universal high-frequency behavior of periodically driven systems: From dynamical stabilization to Floquet engineering, Adv. Phys. **64**, 139 (2015).
[8] A. Eckardt, Atomic quantum gases in periodically driven optical lattices, arXiv:1606.08041.
[9] A. Eckardt and E. Anisimovas, High-frequency approximation for periodically driven quantum systems from a Floquet-space perspective, New J. Phys. **17**, 093039 (2015).
[10] M. M. Maricq, Application of average Hamiltonian theory to the NMR of solids, Phys. Rev. B **25**, 6622 (1982).
[11] T. P. Grozdanov and M. J. Raković, Quantum system driven by rapidly varying periodic perturbation, Phys. Rev. A **38**, 1739 (1988).
[12] S. Rahav, I. Gilary, and S. Fishman, Effective Hamiltonians for periodically driven systems, Phys. Rev. A **680**, 13820 (2003).
[13] C. E. Creffield and F. Sols, Controlled generation of coherent matter currents using a periodic driving field, Phys. Rev. Lett. **100**, 250402 (2008).
[14] N. Goldman and J. Dalibard, Periodically driven quantum systems: Effective Hamiltonians and engineered gauge fields, Phys. Rev. X **4**, 031027 (2014).

[15] N. Goldman, J. Dalibard, M. Aidelsburger, and N. R. Cooper, Periodically-driven quantum matter: The case of resonant modulations, Phys. Rev. A **91**, 033632 (2015).

[16] F. Grossman, T. Dittrich, P. Jung, and P. Hänggi, Coherent destruction of tunneling, Phys. Rev. Lett. **67**, 516 (1991).

[17] C. E. Creffield and G. Platero, Localization of two interacting electrons in quantum dot arrays driven by an ac field, Phys. Rev. B **69**, 165312 (2004).

[18] A. Gómez-León and G. Platero, Charge localization and dynamical spin locking in double quantum dots driven by ac magnetic fields, Phys. Rev. B **84**, 121310 (2011).

[19] G. Platero and R. Aguado, Photon-assisted transport in semiconductor nanostructures, Phys. Rep. **395**, 1 (2004).

[20] C. Sias et al., Observation of photon-assisted tunneling in optical lattices, Phys. Rev. Lett. **100**, 040404 (2008).

[21] R. Ma, M. E. Tai, P. M. Preiss, W. S. Bakr, J. Simon, and M. Greiner, Photon-assisted tunneling in a biased strongly correlated Bose gas, Phys. Rev. Lett. **107**, 095301 (2011).

[22] J. Inoue and A. Tanaka, Photoinduced transition between conventional and topological insulators in two-dimensional electronic systems, Phys. Rev. Lett. **105**, 017401 (2010).

[23] N. H. Lindner, G. Refael, and V. Galitski, Floquet topological insulator in semiconductor quantum wells, Nat. Phys. **7**, 490 (2011).

[24] A. Gómez-León and G. Platero, Floquet-Bloch theory and topology in periodically driven lattices, Phys. Rev. Lett. **110**, 200403 (2013).

[25] P. Delplace, A. Gómez-León, and G. Platero, Merging of Dirac points and Floquet topological transitions in ac-driven graphene, Phys Rev. B **88**, 245422 (2013).

[26] A. G. Grushin, A. Gómez-León, and T. Neupert, Floquet fractional chern insulators, Phys. Rev. Lett. **112**, 156801 (2014).

[27] A. Gómez-León, P. Delplace, and G. Platero, Engineering anomalous quantum Hall plateaus and antichiral states with ac fields, Phys Rev. B **89**, 205408 (2014).

[28] M. Thakurathi, A. A. Patel, D. Sen, and A. Dutta, Floquet generation of Majorana end modes and topological invariants, Phys. Rev. B **88**, 155133 (2013).

[29] M. Benito, A. Gómez-León, V. M. Bastidas, T. Brandes, and G. Platero, Floquet engineering of long-range p-wave superconductivity, Phys. Rev. B **90**, 205127 (2014).

[30] A. Y. Kitaev, Unpaired Majorana fermions in quantum wires, Phys. Usp. **44**, 131 (2001).

[31] V. Mourik, K. Zuo, S. M. Frolov, S. R. Plissard, E. P. A. M. Bakkers, and L. P. Kouwenhoven, Signatures of Majorana fermions in hybrid superconductor-semiconductor nanowire devices, Science **336**, 1003 (2012).

[32] L. P. Rokhinson, X. Liu, and J. K. Furdyna, The fractional a.c. Josephson effect in a semiconductor-superconductor nanowire as a signature of Majorana particles, Nat. Phys. **8**, 795 (2012).

[33] A. Das, Y. Ronen, Y. Most, Y. Oreg, M. Heiblum, and H. Shtrikman, Zero-bias peaks and splitting in an Al-InAs nanowire topological superconductor as a signature of Majorana fermions, Nat. Phys. **8**, 887 (2012).

[34] M. T. Deng, C. L. Yu, G. Y. Huang, M. Larsson, P. Caroff, and H. Q. Xu, Anomalous zero-bias conductance peak in a Nb-InSb nanowire-Nb hybrid device, Nano Lett. **12**, 6414 (2012).

[35] S. Nadj-Perge et al., Observation of Majorana fermions in ferromagnetic atomic chains on a superconductor, Science **346**, 602 (2014).

[36] Y. Oreg, G. Refael, and F. von Oppen, Helical liquids and Majorana bound states in quantum wires, Phys. Rev. Lett. **105**, 177002 (2010).

[37] R. M. Lutchyn, J. D. Sau, and S. D. Sarma, Majorana fermions and a topological phase transition in semiconductor-superconductor heterostructures, Phys. Rev. Lett. **105**, 077001 (2010).

[38] D. E. Liu, A. Levchenko, and H. U. Baranger, Floquet Majorana fermions for topological qubits in superconducting devices and cold-atom systems, Phys. Rev. Lett. **111**, 047002 (2013).

[39] A. Kundu and B. Seradjeh, Transport signatures of Floquet Majorana fermions in driven topological superconductors, Phys. Rev. Lett. **111**, 136402 (2013).

[40] P. Wang, Q. F. Sun, and X. C. Xie, Transport properties of Floquet topological superconductors at the transition from the topological phase to the Anderson localized phase, Phys. Rev. B **90**, 155407 (2014).

[41] S. Blanes, F. Casas, J. Oteo, and J. Ros, The Magnus expansion and some of its applications, Phys. Rep. **470**, 151 (2009).

[42] F. W. J. Olver, D. W. Lozier, R. F. Boisvert, and C. W. Clark, *NIST Handbook of Mathematical Functions* (Cambridge University Press, New York, 2010).

[43] G. A. Watson, *Treatise on the Theory of Bessel Functions* (Cambridge University Press, New York, 1944).

[44] S. W. Li, Z. Z. Li, C. Y. Cai, and C. P. Sun, Probing zero modes of a defect in a Kitaev quantum wire, Phys. Rev. B **89**, 134505 (2014).

[45] Y. Niu, S. B. Chung, C. H. Hsu, I. Mandal, S. Raghu, and S. Chakravarty, Majorana zero modes in a quantum Ising chain with longer-ranged interactions, Phys. Rev. B **85**, 035110 (2012).

[46] E. Lieb, T. Schultz, and D. Mattis, Two soluble models of an antiferromagnetic chain, Ann. Phys. **466**, 407 (1961).

[47] W. DeGottardi, M. Thakurathi, S. Vishveshwara, and D. Sen, Majorana fermions in superconducting wires: Effects of long-range hopping, broken time-reversal symmetry, and potential landscapes, Phys. Rev. B **88**, 165111 (2013).

[48] J. D. Sau and S. D. Sarma, Nat. Commun. **3**, 964 (2012).